HHS Public Access

Author manuscript

Nat Neurosci. Author manuscript; available in PMC 2012 July 01.

Published in final edited form as:

Nat Neurosci. ; 15(1): 131–137. doi:10.1038/nn.2943.

The Na^+/Ca^{2+} exchanger NCKX4 governs termination and adaptation of the mammalian olfactory response

Aaron B. Stephan[1,2], **Steven Tobochnik**[1], **Michele Dibattista**[3], **Crystal M. Wall**[1], **Johannes Reisert**[3], and **Haiqing Zhao**[1]

[1]Department of Biology, The Johns Hopkins University, 3400 N. Charles Street, Baltimore, MD 21218

[3]Monell Chemical Senses Center, 3500 Market Street, Philadelphia, PA 19104

Abstract

Sensory perception requires accurate encoding of stimulus information by sensory receptor cells. Here, we identify NCKX4, a potassium – dependent Na^+/Ca^{2+} exchanger, to be necessary for rapid response termination and proper adaptation of vertebrate olfactory sensory neurons (OSNs). *Nckx4*$^{-/-}$ mouse OSNs display substantially prolonged responses and stronger adaptation. Single – cell electrophysiological analyses demonstrate that the majority of Na^+ – dependent Ca^{2+} exchange in OSNs relevant to sensory transduction is due to NCKX4 and that *Nckx4*$^{-/-}$ mouse OSNs are deficient in encoding action potentials upon repeated stimulation. Olfactory – specific *Nckx4* knockout mice have a reduced ability to locate an odorous source and lower body weights. These results establish the role of NCKX4 in shaping olfactory responses and suggest that rapid response termination and proper adaptation of peripheral sensory receptor cells tune the sensory system for optimal perception.

INTRODUCTION

Accurate encoding of spatial and temporal properties of sensory stimuli by peripheral sensory receptor cells is a prerequisite for accurate sensory perception. Tight and fast regulation of sensory transduction is necessary for the proper activation, termination, and adaptation of sensory responses, with Ca^{2+} often playing a critical role in all three processes. In rod and cone photoreceptors, changes in cytoplasmic Ca^{2+} levels are responsible for regulating the sensitivity and kinetics of phototransduction to background light [1], while in

Correspondence should be addressed to H.Z. (hzhao@jhu.edu).

[2]Current address: Division of Biological Sciences, Cell and Developmental Biology Section, University of California San Diego, La Jolla, CA 92093-0116.

The authors do not declare any competing interests.

A.B.S and H.Z. designed and performed the initial experiments to identify NCKX4. A.B.S generated the targeted deletion of *Nckx4* in mice and designed and conducted the *in situ* hybridizations, immunostaining, EOG analyses, and behavioral analyses. S.T. set up crosses and weighed the conditional knockout mice, performed the OB NCAM staining, and performed the adaptation time course EOGs. J.R. designed and performed the single cell – recordings. M.D. performed the Ca^{2+} – free single – cell recordings. C.M.W. analyzed glomerular formation using anti – OR antibodies (data not shown). A.B.S., H.Z., and J.R. wrote the initial manuscript draft. All authors discussed the results and the contents of the manuscript.

vertebrate olfactory sensory neurons (OSNs), Ca^{2+} plays dual yet seemingly opposing roles in the signaling cascade [2, 3]. Upon odorant stimulation, Ca^{2+} enters OSN cilia through the olfactory cyclic nucleotide – gated (CNG) cation channel, which is opened via the olfactory G – protein mediated signal transduction cascade [2, 3]. Ca^{2+} in OSN cilia triggers a depolarizing Cl^- current, which serves as an amplification step for membrane depolarization [4–6]. Ca^{2+} also adapts the transduction pathway presumably by negatively regulating the activities of several transduction components, which leads to reduced sensitivity to repeated odor exposure [7]. The time course over which cilial Ca^{2+} accumulates and is removed influences not only the sensitivity but also the rates of activation and termination of the olfactory signaling pathway. Thus, proper regulation of cilial Ca^{2+} dynamics should be critical for encoding olfactory stimuli.

Since OSN cilia do not contain intracilial vesicular organelles [8], Ca^{2+} homeostasis is believed to be achieved by plasma membrane Ca^{2+} transporters, including ATP – dependent Ca^{2+} pumps and Na^+/Ca^{2+} exchangers [2, 9]. Na^+/Ca^{2+} exchangers are transmembrane proteins that harness the energy stored within the Na^+ electrochemical gradient across the plasma membrane to actively transfer Ca^{2+} against its electrochemical gradient. There are three families of Na^+/Ca^{2+} exchangers in mammals [10]. The SLC8 family contains three NCX proteins, which exchange 3 Na^+ for one Ca^{2+}. The SLC24 family contains five NCKX proteins, which exchange 4 Na^+ for one Ca^{2+} and one K^+. The CCX family contains one member, NCLX, which is largely uncharacterized. Both NCXs and NCKXs are known to play critical roles in regulating compartmental cytoplasmic Ca^{2+} in sensory receptor cells, particularly in vertebrate [11] and *Drosophila* [12] photoreceptors. Na^+ – dependent Ca^{2+} exchange has been observed in OSNs electrophysiologically and by Ca^{2+} – imaging [13–17]. Inhibition of Na^+/Ca^{2+} exchange in OSNs by replacement of extracellular Na^+ results in prolonged receptor currents due to prolonged elevation of intracilial Ca^{2+} and continuous activation of the Cl^- channel, and low extracellular Na^+ also cause stronger adaptation, suggesting the importance of Na^+/Ca^{2+} exchangers in regulating olfactory transduction [13, 14, 17]. Expression of several Na^+/Ca^{2+} exchangers including members of both NCX and NCKX families has been reported in OSNs [9, 15]. However, the molecular identity of the particular Na^+/Ca^{2+} exchanger(s) involved in olfactory transduction is still undetermined.

In this study, we identified NCKX4 (SLC24a4) to be the principal Na^+/Ca^{2+} exchanger that governs response termination kinetics and adaptation of the OSN, and that subsequently influences how odor information is encoded and perceived.

RESULTS

Nckx4 is expressed specifically in OSNs

We previously conducted a proteomic screen of OSN cilial membranes to identify novel olfactory signaling components [18]. In this screen, a single Na^+/Ca^{2+} exchanger, NCKX4 (SLC24a4), was identified. To determine the expression pattern of *Nckx4* in the olfactory epithelium, we performed *in situ* hybridization and found that *Nckx4* mRNA is expressed specifically in the layer of mature OSNs (Fig. 1a). Consistent with these findings, previous microarray evidence indicated that *Nckx4* was the only Na^+/Ca^{2+} exchanger to be enriched

substantially in the olfactory epithelium [19], and specifically in OSNs [20]. Together, these data implicated NCKX4 to be the leading candidate Na^+/Ca^{2+} exchanger for regulating the OSN response.

Generation of *Nckx4*$^{-/-}$ mice

To determine the function of NCKX4 in the olfactory system, we generated mutant mice for the *Nckx4* gene. We flanked exon 5, which encodes the first of two ion – exchanger domains, with *loxP* sequences. Cre recombinase – mediated deletion of this highly conserved exon also causes a frame shift in the remaining transcript sequence, and should therefore cause a functionally null mutation of NCKX4 (Supplementary Fig.1a – c). Straight knockout (*Nckx4*$^{-/-}$) mice, generated by early embryonic Cre expression, were viable. The deletion of exon 5 from *Nckx4* transcripts was confirmed by RT PCR analysis from *Nckx4*$^{-/-}$ olfactory epithelium cDNA (Fig. 1b). We found that loss of NCKX4 did not affect the overall histology of the olfactory epithelium; the relative proportion of mature (olfactory marker protein positive) and immature (GAP – 43 positive) OSNs was unchanged, and no observable difference in OSN proliferation or death was detected as assessed by EdU nucleotide incorporation and activated Caspase – 3, respectively (Fig. 1c and Supplementary Fig. 1d). Further, the cilial localization of the olfactory transduction components Adenylyl Cyclase III (ACIII) and the B1 subunit of the CNG channel (CNGB1b) were unaltered (Fig. 1d). We also found that the loss of NCKX4 did not affect the overall histology of the olfactory bulb; the total number of glomeruli remained unchanged (Supplementary Fig.1e – f).

Nckx4$^{-/-}$ OSNs exhibit slowed response termination

To analyze the effect of NCKX4 loss on OSN responses, we recorded the electroolfactogram (EOG), an extracellular field potential at the surface of the olfactory epithelium resulting from a summation of individual OSN responses [21, 22]. Upon stimulation with a brief (100 msec) odorant pulse, wildtype EOG signals show a rapid activation phase followed by a termination phase. The signals peak within several hundred milliseconds and recover to baseline within seconds [23, 24]. The peak amplitudes and activation kinetics of EOG signals reflect the overall sensitivity of OSNs. We found that *Nckx4*$^{-/-}$ mice had peak EOG amplitudes equal to wildtype mice across all odorant concentrations to two commonly used odorants, heptanal (Fig. 2a, b) and amyl acetate (Supplementary Fig. 2a, b). We found that the response latency and the time to peak – two metrics for EOG activation kinetics – were unchanged in *Nckx4*$^{-/-}$ mice (Fig. 2c – e). Similar results were seen for responses to amyl acetate (Supplementary Fig. 2c – e). Because both the response amplitude and the activation kinetics were unaffected in the mutant mice, NCKX4 is unlikely to control the sensitivity of OSNs in response to a single odorant exposure.

While *Nckx4*$^{-/-}$ mice showed normal sensitivity, they exhibited remarkably slowed termination kinetics of EOG signals (Fig. 2c, f and Supplementary Fig. 2c, f). The time constants (τ) of the EOG termination phase, obtained by fitting the traces to a single exponential equation, were 2 – 3 – fold longer in *Nckx4*$^{-/-}$ mice as compared to their wildtype littermates. Furthermore, even *Nckx4*$^{+/-}$ (heterozygous) mice showed significantly prolonged termination to stimulation at odorant concentrations near the EC_{50} (Fig. 2c, f and

Supplementary Fig. 2c, f), suggesting a gene dose – dependence for controlling the response termination rate.

We further analyzed the effect of NCKX4 loss on OSN response termination using single – cell suction recordings. The cell bodies of single dissociated OSNs were sucked into a recording pipette electrode with only the cilia and the dendritic knob exposed to a controlled extracellular solution [17]. IBMX (1 mM), a phosphodiesterase inhibitor that elevates cilial cAMP levels, was applied to mimic odorant stimulation and induced rapidly increasing receptor currents in both wildtype and *Nckx4*$^{-/-}$ OSNs (Fig. 3a). IBMX has been widely used as a surrogate for odorants in OSN single – cell studies due to the low probability of a given OSN being responsive to a given odorant. It has been shown that termination kinetics of OSN response under IMBX stimulation closely resemble that under odorant stimulation [25]. In wildtype OSNs, the current in regular Ringer solution recovered to baseline within a short time period after IBMX removal (τ_{Ringer} = 146 ± 13 msec, mean ± s.e.m.) (Fig. 3a, b). In contrast, in *Nckx4*$^{-/-}$ OSNs, the current recovered over a significantly longer time period (τ_{Ringer} = 612 ± 53 msec) (Fig. 3a, b), consistent with the EOG data.

Together, our results demonstrate that NCKX4 is necessary for efficient termination of the olfactory signaling cascade.

NCKX4 is the principal olfactory Na^+/Ca^{2+} exchanger

We next examined whether other Na^+/Ca^{2+} exchangers in addition to NCKX4 also regulate OSN response termination. Single – cell suction recording allows precise inhibition of Na^+/Ca^{2+} exchange [17] by switching the extracellular bath solution to a Na^+ – free solution (Na^+ was replaced equimolarly with choline$^+$, which does not support Na^+/Ca^{2+} exchange) to eliminate all Na^+ – dependent Ca^{2+} extrusion. When wildtype OSNs were switched to a Na^+ – free solution immediately after IBMX stimulation, the termination phase was greatly prolonged ($\tau_{Na-free}$ = 600 ± 71 msec) (Fig. 3a, b) (see also ref. [17]). This prolonged current component is due to slowed Ca^{2+} extrusion and hence prolonged elevated cilial Ca^{2+} and continued opening of the Ca^{2+} – activated Cl^- channel [14, 26]. In contrast, the already prolonged response termination phase of *Nckx4*$^{-/-}$ OSNs was prolonged further only slightly (albeit significantly, see below) by removal of external Na^+ ($\tau_{Na-free}$ = 646 ± 55 msec) (Fig. 3a, b), suggesting that NCKX4 contributes the vast majority of Na^+/Ca^{2+} exchange to regulate OSN response termination. Because response termination can vary largely between individual OSNs, we plotted τ_{Ringer} against $\tau_{Na-free}$ for each OSN. The $\tau_{Na-Free}/\tau_{Ringer}$ ratio remained quite constant among wildtype OSNs, as well as among *Nckx4*$^{-/-}$ OSNs (Fig. 3c). We further calculated the $\tau_{Na-Free}/\tau_{Ringer}$ for each OSN and calculated the average for all wildtype and *Nckx4*$^{-/-}$ OSNs. Exposure to Na^+ – free solution prolonged the response 4.5 ± 0.6 (mean ± s.e.m.) fold in wildtype OSNs but only 1.08 ± 0.03 fold in *Nckx4*$^{-/-}$ OSNs ($P < 0.001$). The slight response prolongation upon Na^+ removal in *Nckx4*$^{-/-}$ OSNs was statistically significant ($P < 0.001$), indicating that a small contribution of other Na^+ – dependent Ca^{2+} extrusion mechanism(s) remains in *Nckx4*$^{-/-}$ OSNs.

Previously, it has been shown that prolonged Ca^{2+} transients in OSNs extend activation of the Ca^{2+} – activated Cl^- channel [14, 17, 26]. To determine whether the effects of prolonged

termination in the *Nckx4* $^{-/-}$ OSNs were indeed dependent on Ca^{2+}, we performed single – cell suction electrode recordings in the presence of regular levels of Ca^{2+} (2 mM) or in low levels of Ca^{2+} (20 μM) within the extracellular solution. This low concentration of Ca^{2+} was chosen to minimize Ca^{2+} influx but not low enough to entirely unblock the CNG channel, which would yield very large Na^+ currents and fast cell deterioration. In wildtype OSNs, the termination τ in the regular Ringer solution (τ = 150 ± 20 msec) and in 20 μM extracellular Ca^{2+} solution (τ =156 ± 30 msec) were comparable (Fig. 3d top, 3e). This result is consistent with the notion that NCKX4 allows an efficient removal of cilial Ca^{2+} and allows proper rate of termination under a broad range of Ca^{2+} concentrations. In *Nckx4*$^{-/-}$ OSNs, the response displayed prolonged termination in comparison to wildtype OSNs both in the regular Ringer solution (τ = 600 ± 90 msec) and in the 20 μM extracellular Ca^{2+} solutions (τ = 288 ± 40 msec), but the termination τ in the 20 μM Ca^{2+} solution was significantly shorter than that in the regular Ringer solution (Fig. 3d bottom, 3e). The less severe defect in 20 μM Ca^{2+} solution in *Nckx4*$^{-/-}$ OSNs is consistent with the idea that there is a smaller amount of Ca^{2+} entering the cilia and activating the Ca^{2+} – activated Cl^- channel. Although the amount of Ca^{2+} entry is reduced in low Ca^{2+} conditions, NCKX4 is still required to ensure a fast response termination.

Together, these results demonstrate that NCKX4 is necessary for nearly all Na^+ – dependent Ca^{2+} exchange that governs OSN response termination, likely by removing cilial Ca^{2+} and thus closing the Ca^{2+} activated Cl^- channel.

Nckx4$^{-/-}$ OSNs over – adapt to repeated odorant exposure

Since Ca^{2+} mediates olfactory adaptation, we hypothesized that NCKX4 is required for OSNs to adapt properly to odor. To test this hypothesis, we performed EOG recordings using a paired – pulse protocol, where the olfactory epithelium was stimulated with two equal 100 – msec odorant pulses. In wildtype mice, the response to the second pulse was significantly reduced relative to the first, signifying that the OSNs were adapted (Fig. 4a – c and Supplementary Fig. 3a – c). In *Nckx4*$^{-/-}$ mice, the response to the second pulse was even further reduced, indicating that *Nckx4*$^{-/-}$ mice exhibited enhanced OSN adaptation (Fig. 4a – c and Supplementary Fig. 3a – c). In wildtype mice, the reduction of the second response largely recovered if the interpulse interval was lengthened to 4 sec or beyond, whereas in *Nckx4*$^{-/-}$ mice significant reduction of the second response was observed even when the interpulse interval was extended to 15 seconds (Supplementary Fig. 3e, f). In addition to an amplitude reduction, another manifestation of adaptation is slower onset kinetics of the EOG signal. Using the metric of onset kinetics, the same phenomenon was seen: OSNs adapt to a greater extent in *Nckx4*$^{-/-}$ mice relative to wildtype (Fig. 4d and Supplementary Fig. 3d). As was seen for the termination kinetics, there was a gene dose dependent effect of NCKX4 on adaptation. *Nckx4*$^{+/-}$ (heterozygotes) showed an adaptation enhancement compared to wildtype, but much less pronounced than *Nckx4*$^{-/-}$ (Fig. 4a – d and Supplementary Fig. 3a – d).

We further characterized the effects of NCKX4 loss on OSN adaptation using single – cell suction pipette recordings. In these experiments, pairs of 1 – sec IBMX (1 mM) stimulations were given with varied interpulse intervals (Fig. 4e). Adaptation was assessed as a reduction

in peak current to the second pulse relative to the first pulse. In both wildtype and *Nckx4*$^{-/-}$ OSNs, the effects of adaptation were strongest when the interpulse interval was shortest and became weaker as the interval was lengthened (Fig. 4f). In *Nckx4*$^{-/-}$ OSNs, the adapted responses were smaller than wildtype for each tested interval, indicating hyper – adaptation. Wildtype OSNs recovered from adaptation within 4 sec after the first pulse (Fig. 4f). In *Nckx4*$^{-/-}$ OSNs, however, the effects of adaptation persisted even when the interpulse interval extended beyond 10 sec (Fig. 4f). Together, these results demonstrate that NCKX4 activity moderates the extent of, and supports recovery from, adaptation to repeated stimulation.

Nckx4$^{-/-}$ OSNs fire fewer action potentials when adapted

The odor – evoked receptor potential is further transduced into action potentials within OSNs, which usually occur during the activation phase of the receptor current [17]. Given that *Nckx4*$^{-/-}$ OSNs displayed slower response termination and stronger adaptation, we asked how this altered receptor potential might affect the encoding of action potentials.

We analyzed the single – cell paired – pulse recordings under a filter setting that allows action currents to be observed (Fig. 5a). Wildtype OSNs quickly regained full ability to generate action potentials when the interpulse period was lengthened; by 0.25 sec after the first stimulation ~45% of OSNs were able to fire action potentials to a second stimulation, and by 2 sec 100% of OSNs fired action potentials (Fig. 5b.) In contrast, *Nckx4*$^{-/-}$ OSNs did not generate any action potentials to the second stimulation until the interpulse interval reached 1 sec and never gained 100% firing probability even after a 10 sec interval (Fig. 5b). These results demonstrate that NCKX4 poises OSNs to relay odor information under adapting stimulation.

Nckx4 $^{-/-}$ mice exhibit a reduced ability to locate odors

Given that *Nckx4*$^{-/-}$ mice displayed a defect in relaying odor information from repeated stimulation, we investigated whether the loss of NCKX4 affects the ability of mice to perceive odors.

We initially observed that *Nckx4*$^{-/-}$ mice weighed less than their wildtype littermates (Fig. 6a, b). In mice, olfaction is required for pups to suckle. Reduced body weight is a hallmark characteristic of olfactory defects in mice due to impaired ability to locate the teat: anosmic mice die within the first few postnatal days unless special care is provided [27–29]. *Nckx4* $^{-/-}$ mice were viable through weaning without special care, thus suggesting that they retain at least some functional olfactory perception. But consistent with an olfactory impairment, they weighed equally to their wildtype littermates at birth and developed defects in body weight during the nursing period. Their body weight defects were most pronounced at the time of weaning (21 – 28 days after birth) and became progressively less pronounced through 4 months of observation (Fig. 6b). To determine whether the body weight reduction was likely due to an olfactory defect rather than pleiotropic effects, we generated olfactory – specific knockout mice, where *Nckx4* was conditionally knocked out by the expression of Cre recombinase under the control of the olfactory marker protein (OMP) promoter [30]. OMP shows restricted expression in sensory neurons of the main olfactory epithelium and of other

olfactory subsystems. EOG recordings of these conditional *Nckx4* knockout mice (*Nckx4*$^{flox/flox}$; *Omp*$^{Cre/+}$) showed the similar response defects found in the straight knockout (*Nckx4*$^{-/-}$) mice (data not shown). We found that the reduced body weight phenotype persisted in these conditional knockout mice (Fig. 6c).

To further test whether slower response termination and enhanced adaptation of OSNs affect the ability of mice to perceive odors, we conducted the Buried Food Pellet Test. In this test, food – restricted wildtype mice learned to rapidly locate a buried food pellet, showing daily performance improvements through 5 trial days (Fig. 6d and Supplementary Movie 1). In contrast, most olfactory conditional *Nckx4* knockout mice failed to locate the buried pellet within the allotted 200 seconds (Fig. 6d and Supplementary Movie 1). Over the course of 5 trial days, these conditional *Nckx4* knockout mice showed no significant improvements in their ability to locate the pellet. Importantly, on trial day 6, when the food pellet was made visible by placing it on the surface, both wildtype and olfactory conditional *Nckx4* knockout mice rapidly located the pellet within a similar time frame, controlling for possible secondary locomotor, motivational, or cognitive defects. These results demonstrate that NCKX4, which confers rapid olfactory response termination and moderates OSN adaptation, is necessary for mice to optimally locate odorous sources.

DISCUSSION

In this study, we identified NCKX4 to be the principal Na^+/Ca^{2+} exchanger to allow rapid response termination and proper adaptation of the OSN, presumably by mediating Ca^{2+} extrusion from OSN cilia. Furthermore, we showed that by modulating the peripheral olfactory response, NCKX4 proves critical for an animal to accurately encode and react to olfactory stimuli in the environment.

NCKX4 is a component of the olfactory transduction pathway

NCKX4 (SLC24a4) was initially chosen as the leading candidate for the olfactory Na^+/Ca^{2+} exchanger based on our previous proteomic analysis aiming to identify novel olfactory transduction components [18]. Historically, molecular identification of many olfactory transduction components was first deduced by the abundance and localization of mRNAs through the use of either cDNA library screening [31–35] or PCR – based approaches [36–38]. Many of these components were later functionally confirmed by gene knockout experiments in mice [23, 28, 29, 39–41]. By directly detecting the proteins at the site of their predicted function, cilial membrane proteomics have proven fruitful in identifying the remaining long – sought olfactory transduction components, including the olfactory Ca^{2+} – activated Cl^- channel ANO2[18] and, here, the olfactory Na^+/Ca^{2+} exchanger NCKX4 (Supplementary Fig. 4).

The *Nckx4* gene was first cloned from human and mouse brains [42], and the NCKX4 protein was demonstrated to display K^+ – dependent Na^+/Ca^{2+} exchanger activity [42, 43]. However, no specific physiological role has been definitively attributed to NCKX4. Through loss – of – function analysis, this current study defines a physiological role for NCKX4 in olfactory transduction. We showed that NCKX4 is required to allow rapid olfactory termination and to prevent over adaptation to repeated stimulation. These effects of NCKX4 are most likely

due to the Ca^{2+} transporter activity of NCKX4. However, one cannot exclude the possibility that NCKX4 may have additional functions in the olfactory system. Future technological improvements that allow imaging of Ca^{2+} dynamics within mammalian olfactory cilia will further clarify the precise function of NCKX4 in olfactory transduction.

It has been suggested that active extrusion of Ca^{2+} from olfactory cilia is mediated by both Na^+/Ca^{2+} exchangers and plasma membrane Ca^{2+} ATPases (PMCAs). Na^+/Ca^{2+} exchangers have been favored as a mechanism for extruding Ca^{2+} from OSNs for olfactory transduction [13, 14, 17]. Na^+/Ca^{2+} exchangers have a much greater capacity to extrude Ca^{2+} than PMCAs [44], and are thus better suited for rapidly reducing intracilial Ca^{2+} to fulfill the need for rapid OSN response kinetics. In comparison to NCX, NCKX proteins harness additional driving force for Ca^{2+} by coupling the transport of an additional Na^+ and a K^+, which can maintain the driving force for Ca^{2+} removal even at depolarized membrane potentials and can allow the reduction of Ca^{2+} to nanomolar levels [45, 46]. NCKX4 is therefore well suited for its role in regulating olfactory responses.

NCKX4 regulates the olfactory response

The loss of NCKX4 could influence the sensitivity of the OSN response positively by increasing Ca^{2+} – activated Cl^- current and negatively by increasing PDE1C activity [23], increasing inhibition of the CNG channel, and loss of the electrogenic effect [47]. However, we found that both amplitude and activation kinetics of the EOG response were, surprisingly, not changed in *Nckx4*$^{-/-}$ mice (Fig. 2). This unchanged sensitivity in *Nckx4*$^{-/-}$ OSNs could result from a cancellation of these positive and negative effects. Alternatively, NCKX4 – mediated Ca^{2+} extrusion might not affect these mechanisms until after the response has peaked, so that the loss of NCKX4 does not alter response sensitivity to a brief odorant exposure.

A pronounced effect of NCKX4 loss is stronger OSN adaptation (Fig. 4 and Fig. 5). This result provides *in vivo* demonstration that Ca^{2+} mediates olfactory adaptation. While it is thought that Ca^{2+} – mediated adaptation is via negative feedback of Ca^{2+} on olfactory signaling components, the exact molecular target(s) of this feedback remain to be determined [24].

The most pronounced effect of NCKX4 loss on the olfactory response is a prolonged termination phase (Fig. 2). Loss of one *Nckx4* allele (*Nckx4*$^{+/-}$) caused a mild prolongation, whereas loss of both *Nckx4* alleles (*Nckx4* $^{-/-}$) caused a severe prolongation. Termination of the OSN response requires the closure of both the CNG channel and the ANO2 channel. Degradation of cAMP by phosphodiesterase 1C (PDE1C), which leads to closure of the CNG channel, was once thought to determine the rate of response termination. However, *Pde1c* $^{-/-}$ mice do not show a prolonged olfactory response, indicating that regulation of cAMP dynamics does not dominate the rate of response termination [23]. The slower termination seen in *Nckx4* $^{-/-}$ mice could be best attributed to a slower clearance of Ca^{2+} from OSN cilia, and thus prolonged activation of the Cl^- current (however, see ref [48]). Together, these studies establish that regulation of Ca^{2+} dynamics, rather than degradation of cAMP, plays the leading role in determining the rate of OSN response termination.

Olfactory behavior requires controlled response kinetics

It has always been assumed that rapid termination of peripheral sensory responses is necessary to prepare animals to sense recurring stimulation. However, in the olfactory system this assumption has never been fully testable due to the fact that most mutations in core and modulatory signal transduction components cause either complete loss [28, 29, 41] or severe reductions in sensitivity of the OSN response [23, 39, 49]. This loss or reduction of OSN sensitivity precluded investigations and confounded interpretations of whether alterations in peripheral response properties affect the ability of animals to encode and react to sensory stimuli.

Ncxk4 knockout mice, which display defects in response termination and adaptation but have unchanged sensitivity, provided a unique opportunity to address this question. We found that defects in termination and adaptation of the OSN receptor potential led to a defect in encoding action potentials (Fig. 5). Further, olfactory – specific *Nckx4* knockout mice displayed lower body weights, which is consistent with a nursing defect due to impaired olfactory function (Fig. 6c). Finally, these mice were less efficient at performing a food – finding task (Fig. 6d). Thus, by identifying NCKX4 as a regulator of OSN responses, these studies suggest that rapid response termination and proper regulation of adaptation in OSNs are essential to properly encode and react to olfactory stimuli.

METHODS

Animals

For all experiments involving mice, the animals were handled and euthanized in accordance with methods approved by the Animal Care and Use Committees of each applicable institution. Unless otherwise noted, all analyses involving animals were performed on adult (> 40 day – old) mice.

Generation of *Nckx4* knockout mice

The 85 bp exon 5 of *Nckx4* gene on chromosome 12 was selected to be flanked by *loxP* sites, with a 4.0 kb fragment upstream and a 5.2 kb fragment downstream of this exon used as homologous arms for ES cell gene targeting. pBluescript KS (Clontech) was PCR amplified with primers ACTGGGCCTGGTCACAGGCCTGTATCTGAAGGGAGAGGTAACAGAGGTGTTACAACGTCGTGACTGGGAA and CTCAAAAAATAAGGGGAAACACAATTGAGGAAACACTGGATAGAGAACTCGTAATACGACTCACTATAGGGC, which contain 50 bp homologous arms (underlined) for the *Nckx4* genomic DNA, and the resulting PCR product was used to retrieve the genomic DNA from BAC RP135 – I1 (Children's Hospital Oakland Research Institute BACPAC Resource Center) in SW102 cells using a cell – based recombineering procedure [50]. A loxP – Neomycin Resistance Cassette – loxP sequence amplified from pL452 with primers CGGTGCCAGGCTCAGATCCACACTGTGTCACTGAGAGCTTTCTGCCATCCGCCCAATTCCGATCATATTC and AGGCAACTGGGTTGTGACAAGGGAGGGGAGCACGCAGCCCCTGGGCAGGTCCGCTCTAGAACTAGTGGA, which contain 50 bp homologous targeting arms, was

recombineered 5′ to Exon 5 within SW102 cells. The neomycin cassette was removed by arabinose – induced Cre recombinase expression in SW106 cells, leaving a single *loxP* sequence upstream of Exon 5. A Frt Neomycin Resistance Cassette – Frt – loxP sequence amplified from pL451 with primers ATGCAGAGAGAGCCAGGGCTGACTGCCCAGGGCAGTGGGGCATTTACCAGCTTGATATCGAATTCCGAAG and TGTCCCTCTGACCCCCTTGGGTTTACAAGTGAGGAAATGGAGACTTGGAGCTAATAA CTTCGTATAGCATAC, which contain 50 bp homologous targeting arms, was recombineered 3′ to Exon 5 within SW102 cells. The targeting vector was assessed by extensive restriction digestion and sequencing analysis.

ES cell gene targeting was performed in a 129s6 SvEv ES cell line (MC1 line, Johns Hopkins University transgenic core). 384 individual clones were screened for homologous recombination using a *pgk* promoter – specific primer CTACTTCCATTTGTCACGTCCTG and upstream primer CTCACATAGGTACTGCTCAACAGAC outside of the 5′ arm. Two ES clones were confirmed with homologous combination: 1A12 and 2B2. Each ES cell clone was injected into blastocysts (JHU transgenic core). The chimeras with highest fraction of agouti fur from both parent ES cell clones were mated to C57BL/6 females (Jackson), and germline transmission was determined in the F1 generation by the presence of agouti fur color and positive PCR for the mutant allele. Only ES clone 2B2 resulted in germline transmission. For germline (straight) knockouts, the F1 heterozygote was mated to the early embryonically – expressing Cre recombinase mouse line B6.FVB – Tg(EIIa – cre)C5379Lmgd/J (The Jackson Laboratory), the F2 mice were back – crossed to C57BL/6 to eliminate the *Cre* allele, and then the F3 mice were inbred to obtain homozygotes. For the OSN – specific conditional knockout mice, the F1 was mated with the ubiquitously – expressing Flippase line 129S4/SvJaeSor – *Gt(ROSA)26Sor*$^{tm1(FLP1)Dym}$/J (The Jackson Laboratory), the F2 mice were back – crossed to C57BL/6 to eliminate the *flp*, the F3 mice were mated with mouse line B6;129P2 – *Omp*$^{tm4(cre)Mom}$/MomJ (*Omp*^{Cre}) (The Jackson Laboratory), and then the F4 mice were inbred to obtain 9 separate genotypes, including *Nckx4*$^{flox/flox}$;*Omp*$^{Cre/+}$, the OSN – specific conditional line. Primers AAAGGAAATGAAGAGAAGGC (AS67), and TCATCTCATAAGAAGCCCAG (AS68), which span the floxed exon 5 region, were used to genotype the *Nckx4* allele, with expected band sizes being 615 bp for wildtype, 823 bp for the floxed exon (Supplementary Fig. 1b), and 450 bp for the knocked – out exon (Supplementary Fig. 1c).

RT – PCR analysis of olfactory epithelium RNA

Total olfactory epithelial RNA was isolated using TRIzol Reagent (Invitrogen). cDNA was made by reverse transcription of total RNA using random decamer primers (Ambion). To amplify each specific gene, lower PCR cycles were used to preserve semi – quantitative information regarding relative transcript abundance. The primers used for *Nckx4* were TCCAACAAAGAACGACAGCA and GTTCCTACACCGACATCTCC (245 bp product with Exon 5, 160 bp without Exon 5), for *Cnga2* were TGCCGTAAGGGGGACATTG and ACAGCACTTCTAACTCCTGGGGTC (596 bp product), for *Ano2* were AGTCATCTGTTTGACAATCCAG and CACTCTCCTTTAACAGTTTCTC (198 bp

product in olfactory tissue), and for *Gapdh* were GGGTGGTGCCAAAAGGGTC and GGAGTTGCTGTTGAAGTCACA (223 bp product).

In situ hybridization

Nckx4 probe template was PCR amplified from mouse olfactory epithelial cDNA with primers TACTACTCGAGCTCTGTCATTGTGCTCATTGCG and AGATGGCGGCCGCCGTGAACACCCACTTAGCCTTGTC, and cloned into pBluescript KS(+) (Clontech). This 655 bp fragment of *Nckx4* was chosen to minimize cross – reactivity of the probe with other Na^+/Ca^{2+} genes. Antisense and sense digoxigenin – labeled RNA probes were then generated by transcription from the T3 and T7 promoters. The *in situ* hybridization was performed on 14 μm thick OE cyrosections.

Immunohistochemistry

The olfactory epithelium (OE) and olfactory bulb tissues were fixed in 4% (wt/vol) paraformaldehyde at 4°C followed by cryoprotection in 30% (wt/vol) sucrose. The tissues were cut into 18 μm – thick (OE), 20 μm – thick (olfactory bulb) coronal cryosections. Sections were incubated at 4°C overnight with primary antibodies in PBS containing 0.1% (vol/vol) Triton X – 100 and 1% (vol/vol) goat serum. Primary antibodies were used at the following dilutions: anti – OMP, 1:1000 (chicken antibody, provided by Q. Gong); anti – Gap43, 1:500 (Chemicon MAB347); anti – ACIII (Chemicon AB3403), 1:200; 1:500; anti – CNGB1b [24], 1:300; anti – NCAM (DSHB, 5B8 supernatant), 1:1. After washing, the sections were incubated with fluorescent secondary antibodies, mounted in Vectashield (Vector Labs) containing DAPI stain and imaged. To assess cell death, 30 μm – thick sections were stained with anti – cleaved Caspase – 3 antibody (Cell Signaling Technology #9661) at a dilution of 1:200 as the primary antibody. The activated Caspase – 3 staining was performed on 28 day – old mice.

Cell proliferation assay

Mice were injected with 125 μg 5 – ethynyl – 2′ deoxyuridine (EdU) (Invitrogen) every 2 hours for 12 hours (7 injections total). Two hours after the final injection, the tissue was fixed and cryoprotected as described above. Olfactory epithelium tissue was cut into 30 μm sections. EdU – labeled cells were detected using Click – iT EdU Alexa Fluor 488 Imaging Kit (Invitrogen). Sections were mounted in Vectashield containing DAPI stain and imaged. The EdU labeling was performed on 28 day – old mice.

EOG recording

Mouse EOG recordings were performed as described [21]. Adult mice, aged 3 – 5 months, were used. Heptanal and amyl acetate and were diluted in DMSO to result in a 50x stock solution series. The stock solutions were then diluted to 1x in water to 5 ml final volume in a sealed 60 ml glass bottle to generate vapor phase odorant. EOGs were recorded from a consistent position on turbinate IIB. One set of mice was used in single – pulse dose – response recordings. Another set of mice was used for single, paired – pulse, and extended – pulse recordings at 10^{-4} and 10^{-3} M odorant concentrations. The data was collected and analyzed using AxoGraph Software (Axon Instruments) at a sampling rate of 1 KHz. All

recordings were digitally filtered at 25 Hz prior to analysis. For measuring termination time constants, the time windows used for the fit were 2.5 – 4 sec for 10^{-7} M odorant, 2.4 – 4 sec for 10^{-6} M, 2.4 – 4.5 sec for 10^{-5} M, 2.4 – 10 sec for 10^{-4} M, 2.4 – 15 s for 10^{-3} M, and 2.4 – 20 sec for 10^{-2} – 0.05 M.

Single – cell suction recording and analysis

The suction pipette technique [17] was used to perform single OSN recordings. The cell body of an isolated OSN was sucked into the tip of a recording pipette, leaving the cilia and the dendritic knob (but not the cell body) accessible for solution changes. Solution exchanges were achieved by transferring the tip of the recording pipette across the interface of neighboring streams of solution using the Perfusion Fast – Step SF – 77B solution changer (Warner Instruments). As the intracellular voltage is free to vary in this recording configuration, the recorded current has two components: fast biphasic current transients resembling action potentials and the slower receptor current. Currents were recorded with a Warner PC – 501A patch clamp amplifier, digitized using a Mikro1401 and Signal acquisition software (Cambridge Electronic Design). Suction currents were sampled at 10 KHz. The recorded signals were filtered DC – 50 Hz to display the suction current alone, and filtered DC – 5000 Hz to display action potential currents. Mammalian Ringer solution contained (in mM): 140 NaCl, 5 KCl, 1 $MgCl_2$, 2 $CaCl_2$, 0.01 EDTA, 10 HEPES, and 10 glucose. The pH was adjusted to 7.5 with NaOH. All chemicals were purchased from Sigma. Experiments were performed at 37°C.

The decay time constant was calculated by integrating the current generated after cessation of IBMX exposure. This overall charge was normalized to the current at the cessation of IBMX exposure. The obtained time constant is mathematically equivalent to the time constant obtained from a single exponential decay (in cases that the current decay follows a single exponential decay).

Body mass measurement

Mouse pups were weighed daily to an accuracy of 10 mg. After weaning, mice were weighed weekly to an accuracy of 100 mg. All weight measurements were carried out at the same time of day.

Buried food pellet test

The Buried Food Pellet Test was performed using adult *Nckx4*$^{+/+}$;*Omp*$^{Cre/+}$ (n = 20) and *Nckx4*$^{flox/flox}$;*Omp*$^{Cre/+}$ (n = 20) mice at Zietgeber Time 7 – 12. All animals were housed individually with wood – shavings bedding for the duration of the experiment with free access to water. Mice were deprived of food for 24 h prior to the experiment and subsequently restricted to 2.5 g of Rodent Chow (Harlan Teklad) per day. The testing chambers were clean cages of dimensions 30 × 19 × 13 (L× W × H, in cm) filled with ~800 cm^3 of wood – shavings bedding. Two 40 – 60 mg pieces of Oreo Cookies (Nabisco) were buried just below the surface of the bedding in the following manner: The cage area was designated into halves length – wise. One cookie piece was buried in a randomized location within the left half, the other within the right half. Including two pellets in the experiment reduced the effective search area by half and better controlled for variance in the depth that

the pellet was buried. In a single trial, a mouse was placed in the center of the cage and was given 200 sec to locate either of the two pellets. Latency in finding the first pellet was recorded when the mouse touched the pellet. After the mouse located the first pellet, they were allowed to consume the cookie, and were given another 200 sec to locate the second pellet. If a mouse failed to find a pellet within the allotted 200 sec, the cookie pellet was exposed and presented to the mouse for subsequent consumption. After the trial, each mouse was returned to its respective cage. Mice were tested in a single trial per day for 5 consecutive days. The testing order of the animals was randomized for each day. Fresh bedding was used for each mouse, each day.

Statistical analyses

For the comparison of percentage of OSNs firing action potentials (Fig. 5b), the *P* – values were calculated using a Chi – square test. For all other comparisons that only involved WT mice vs. *Nckx4*$^{-/-}$ mice, *P* – values were calculated with Student's *t* – test at each odorant concentration or timepoint. When three or more genotypes were compared, pairwise *P* – values were calculated with the Tukey – Kramer ANOVA post – test at each odorant concentration or timepoint. Statistical analyses were performed using R (http://www.r-project.org/).

Supplementary Material

Refer to Web version on PubMed Central for supplementary material.

Acknowledgments

We thank T. Bozza for providing the OMP – Cre mouse line. We thank K. Cunningham, K. Cygnar, D. Fambrough, S. Hattar, R. Kuruvilla, D. Luo, and F. Margolis for suggestions and discussions. We also thank members of the Hattar – Kuruvilla – Zhao mouse tri – lab of the Johns Hopkins Department of Biology for discussions. This research is supported by NIH DC007395, a Morley Kare Fellowship (to J.R.) and the Monell Chemical Senses Center. A.B.S. is currently a Department of Energy-Biosciences Fellow of the Life Sciences Research Foundation.

References

1. Fain GL, Matthews HR, Cornwall MC, Koutalos Y. Adaptation in vertebrate photoreceptors. Physiol Rev. 2001; 81:117–151. [PubMed: 11152756]
2. Kleene SJ. The electrochemical basis of odor transduction in vertebrate olfactory cilia. Chem Senses. 2008; 33:839–859. [PubMed: 18703537]
3. Kaupp UB. Olfactory signalling in vertebrates and insects: differences and commonalities. Nat Rev Neurosci. 2010; 11:188–200. [PubMed: 20145624]
4. Reisert J, Lai J, Yau KW, Bradley J. Mechanism of the excitatory Cl- response in mouse olfactory receptor neurons. Neuron. 2005; 45:553–561. [PubMed: 15721241]
5. Lowe G, Gold GH. Nonlinear amplification by calcium-dependent chloride channels in olfactory receptor cells. Nature. 1993; 366:283–286. [PubMed: 8232590]
6. Kleene SJ. High-gain, low-noise amplification in olfactory transduction. Biophys J. 1997; 73:1110–1117. [PubMed: 9251827]
7. Zufall F, Leinders-Zufall T. The cellular and molecular basis of odor adaptation. Chem Senses. 2000; 25:473–481. [PubMed: 10944513]
8. Menco BP. Ciliated and microvillous structures of rat olfactory and nasal respiratory epithelia. A study using ultra-rapid cryo-fixation followed by freeze-substitution or freeze-etching. Cell Tissue Res. 1984; 235:225–241. [PubMed: 6367994]

9. Pyrski M, et al. Sodium/calcium exchanger expression in the mouse and rat olfactory systems. J Comp Neurol. 2007; 501:944–958. [PubMed: 17311327]
10. Lytton J. Na+/Ca2+ exchangers: three mammalian gene families control Ca2+ transport. Biochem J. 2007; 406:365–382. [PubMed: 17716241]
11. Schnetkamp PP. Calcium homeostasis in vertebrate retinal rod outer segments. Cell Calcium. 1995; 18:322–330. [PubMed: 8556771]
12. Wang T, et al. Light activation, adaptation, and cell survival functions of the Na+/Ca2+ exchanger CalX. Neuron. 2005; 45:367–378. [PubMed: 15694324]
13. Antolin S, Matthews HR. The effect of external sodium concentration on sodium-calcium exchange in frog olfactory receptor cells. J Physiol. 2007; 581:495–503. [PubMed: 17379630]
14. Reisert J, Matthews HR. Na+-dependent Ca2+ extrusion governs response recovery in frog olfactory receptor cells. J Gen Physiol. 1998; 112:529–535. [PubMed: 9806962]
15. Noe J, Tareilus E, Boekhoff I, Breer H. Sodium/calcium exchanger in rat olfactory neurons. Neurochem Int. 1997; 30:523–531. [PubMed: 9152993]
16. Jung A, Lischka FW, Engel J, Schild D. Sodium/calcium exchanger in olfactory receptor neurones of Xenopus laevis. Neuroreport. 1994; 5:1741–1744. [PubMed: 7827321]
17. Reisert J, Matthews HR. Response properties of isolated mouse olfactory receptor cells. J Physiol. 2001; 530:113–122. [PubMed: 11136863]
18. Stephan AB, et al. ANO2 is the cilial calcium-activated chloride channel that may mediate olfactory amplification. Proc Natl Acad Sci U S A. 2009; 106:11776–11781. [PubMed: 19561302]
19. Su AI, et al. A gene atlas of the mouse and human protein-encoding transcriptomes. Proc Natl Acad Sci U S A. 2004; 101:6062–6067. [PubMed: 15075390]
20. Sammeta N, Yu TT, Bose SC, McClintock TS. Mouse olfactory sensory neurons express 10,000 genes. J Comp Neurol. 2007; 502:1138–1156. [PubMed: 17444493]
21. Cygnar KD, Stephan AB, Zhao H. Analyzing responses of mouse olfactory sensory neurons using the air-phase electroolfactogram recording. J Vis Exp. 2010; 37
22. Scott JW, Scott-Johnson PE. The electroolfactogram: a review of its history and uses. Microsc Res Tech. 2002; 58:152–160. [PubMed: 12203693]
23. Cygnar KD, Zhao H. Phosphodiesterase 1C is dispensable for rapid response termination of olfactory sensory neurons. Nat Neurosci. 2009; 12:454–462. [PubMed: 19305400]
24. Song Y, et al. Olfactory CNG channel desensitization by Ca2+/CaM via the B1b subunit affects response termination but not sensitivity to recurring stimulation. Neuron. 2008; 58:374–386. [PubMed: 18466748]
25. Reisert J, Yau KW, Margolis FL. Olfactory marker protein modulates the cAMP kinetics of the odour-induced response in cilia of mouse olfactory receptor neurons. J Physiol. 2007; 585:731–740. [PubMed: 17932148]
26. Reisert J, Matthews HR. Simultaneous recording of receptor current and intraciliary Ca2+ concentration in salamander olfactory receptor cells. J Physiol. 2001; 535:637–645. [PubMed: 11559763]
27. Zhao H, Reed RR. X inactivation of the OCNC1 channel gene reveals a role for activity-dependent competition in the olfactory system. Cell. 2001; 104:651–660. [PubMed: 11257220]
28. Wong ST, et al. Disruption of the type III adenylyl cyclase gene leads to peripheral and behavioral anosmia in transgenic mice. Neuron. 2000; 27:487–497. [PubMed: 11055432]
29. Belluscio L, Gold GH, Nemes A, Axel R. Mice deficient in G(olf) are anosmic. Neuron. 1998; 20:69–81. [PubMed: 9459443]
30. Li J, Ishii T, Feinstein P, Mombaerts P. Odorant receptor gene choice is reset by nuclear transfer from mouse olfactory sensory neurons. Nature. 2004; 428:393–399. [PubMed: 15042081]
31. Yan C, et al. Molecular cloning and characterization of a calmodulin-dependent phosphodiesterase enriched in olfactory sensory neurons. Proc Natl Acad Sci U S A. 1995; 92:9677–9681. [PubMed: 7568196]
32. Sautter A, Zong X, Hofmann F, Biel M. An isoform of the rod photoreceptor cyclic nucleotide-gated channel beta subunit expressed in olfactory neurons. Proc Natl Acad Sci U S A. 1998; 95:4696–4701. [PubMed: 9539801]

33. Jones DT, Reed RR. Golf: an olfactory neuron specific-G protein involved in odorant signal transduction. Science. 1989; 244:790–795. [PubMed: 2499043]
34. Dhallan RS, Yau KW, Schrader KA, Reed RR. Primary structure and functional expression of a cyclic nucleotide-activated channel from olfactory neurons. Nature. 1990; 347:184–187. [PubMed: 1697649]
35. Bakalyar HA, Reed RR. Identification of a specialized adenylyl cyclase that may mediate odorant detection. Science. 1990; 250:1403–1406. [PubMed: 2255909]
36. Liman ER, Buck LB. A second subunit of the olfactory cyclic nucleotide-gated channel confers high sensitivity to cAMP. Neuron. 1994; 13:611–621. [PubMed: 7522482]
37. Buck L, Axel R. A novel multigene family may encode odorant receptors: a molecular basis for odor recognition. Cell. 1991; 65:175–187. [PubMed: 1840504]
38. Bradley J, Li J, Davidson N, Lester HA, Zinn K. Heteromeric olfactory cyclic nucleotide-gated channels: a subunit that confers increased sensitivity to cAMP. Proc Natl Acad Sci U S A. 1994; 91:8890–8894. [PubMed: 7522325]
39. Munger SD, et al. Central role of the CNGA4 channel subunit in Ca2+-calmodulin-dependent odor adaptation. Science. 2001; 294:2172–2175. [PubMed: 11739959]
40. Michalakis S, et al. Loss of CNGB1 protein leads to olfactory dysfunction and subciliary cyclic nucleotide-gated channel trapping. J Biol Chem. 2006; 281:35156–35166. [PubMed: 16980309]
41. Brunet LJ, Gold GH, Ngai J. General anosmia caused by a targeted disruption of the mouse olfactory cyclic nucleotide-gated cation channel. Neuron. 1996; 17:681–693. [PubMed: 8893025]
42. Li XF, Kraev AS, Lytton J. Molecular cloning of a fourth member of the potassium-dependent sodium-calcium exchanger gene family, NCKX4. J Biol Chem. 2002; 277:48410–48417. [PubMed: 12379639]
43. Visser F, Valsecchi V, Annunziato L, Lytton J. Exchangers NCKX2, NCKX3, and NCKX4: identification of Thr-551 as a key residue in defining the apparent K(+) affinity of NCKX2. J Biol Chem. 2007; 282:4453–4462. [PubMed: 17172467]
44. Blaustein MP, Lederer WJ. Sodium/calcium exchange: its physiological implications. Physiol Rev. 1999; 79:763–854. [PubMed: 10390518]
45. Schnetkamp PP, Basu DK, Szerencsei RT. The stoichiometry of Na-Ca+K exchange in rod outer segments isolated from bovine retinas. Ann N Y Acad Sci. 1991; 639:10–21. [PubMed: 1785833]
46. Altimimi HF, Schnetkamp PP. Na+/Ca2+-K+ exchangers (NCKX): functional properties and physiological roles. Channels (Austin). 2007; 1:62–69. [PubMed: 18690016]
47. Danaceau JP, Lucero MT. Electrogenic Na(+)/Ca(2+) exchange. A novel amplification step in squid olfactory transduction. J Gen Physiol. 2000; 115:759–768. [PubMed: 10828249]
48. Billig GM, Pal B, Fidzinski P, Jentsch TJ. Ca(2+)-activated Cl(-) currents are dispensable for olfaction. Nat Neurosci. 2011; 14:763–769. [PubMed: 21516098]
49. Buiakova OI, et al. Olfactory marker protein (OMP) gene deletion causes altered physiological activity of olfactory sensory neurons. Proc Natl Acad Sci U S A. 1996; 93:9858–9863. [PubMed: 8790421]
50. Liu P, Jenkins NA, Copeland NG. A highly efficient recombineering-based method for generating conditional knockout mutations. Genome Res. 2003; 13:476–484. [PubMed: 12618378]

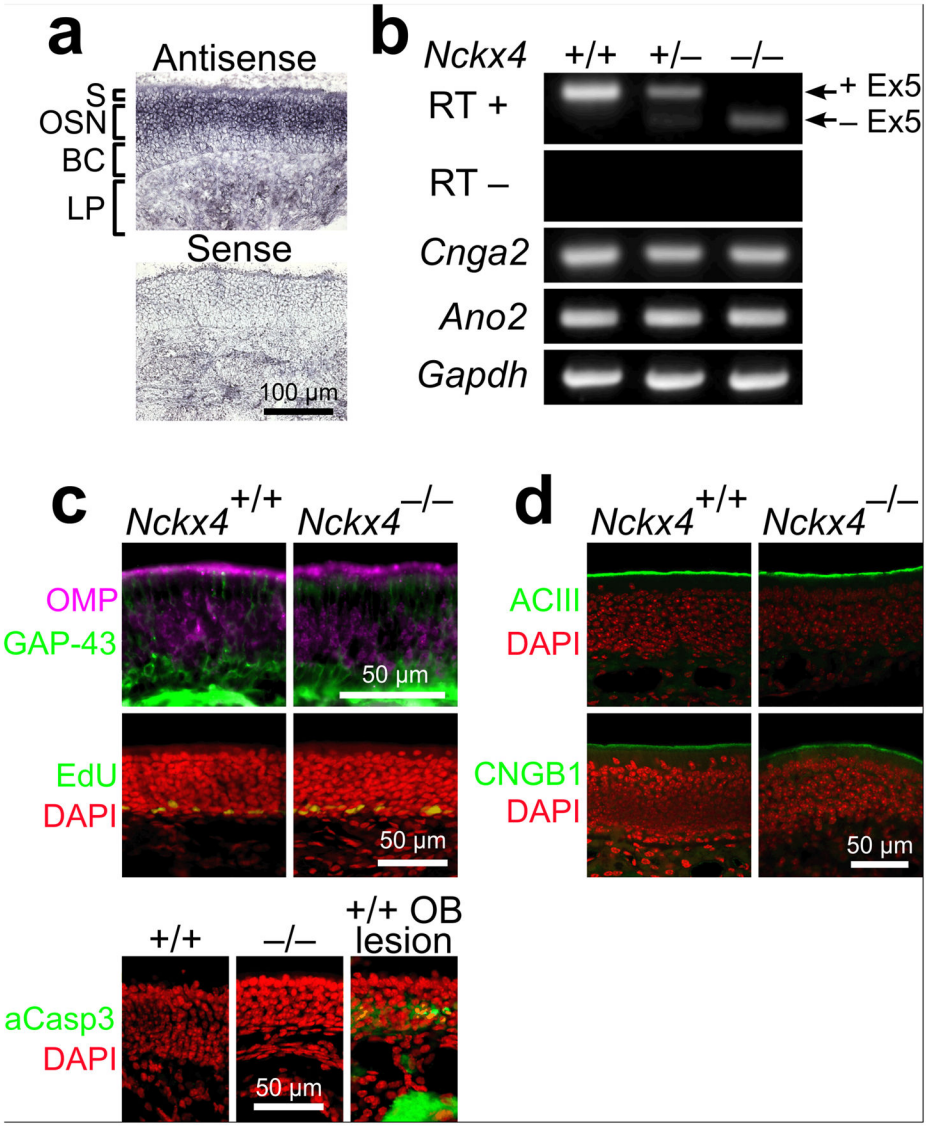

Figure 1. Expression of *Nckx4* in the olfactory epithelium and the effects of NCKX4 loss on other olfactory transduction components

(**a**) *in situ* hybridization showing *Nckx4* mRNA localization within the mouse olfactory epithelium. S, sustentacular cell layer; OSN, olfactory sensory neuron layer; BC, basal cell layer; LP, lamina propria.

(**b**) RT – PCR analysis of *Nckx4* mRNA in WT, *Nckx4*$^{+/-}$, and *Nckx4*$^{-/-}$ mice. The amplified region flanks the targeted Exon 5. Amplifications of *Cnga2*, *Ano2*, and *Gapdh* transcripts were used as loading controls. See Supplementary Figure 1a – c for details of the gene targeting.

(**c**) Top panels: immunostaining in olfactory epithelium sections for OMP, a marker of mature OSNs, and GAP – 43, a marker of immature OSNs. Middle panels: labeling by EdU, a nucleotide analog incorporated during mitosis. The nuclei are stained with DAPI. See Supplementary Figure 1d for cell counts. Bottom panels: immunostaining for activated Caspase – 3, an indicator of apoptosis. Fewer than one labeled cell per cryosection was

visible for WT and *Nckx4*$^{-/-}$ mice, whereas labeled cells and axon bundles were apparent in the positive control olfactory epithelium (48 hr after lesioning the olfactory bulb). The nuclei are stained with DAPI.

(**d**) Immunostaining in olfactory epithelium sections for the olfactory transduction components ACIII (upper panel) and CNGB1b (lower panel). The nuclei are stained with DAPI.

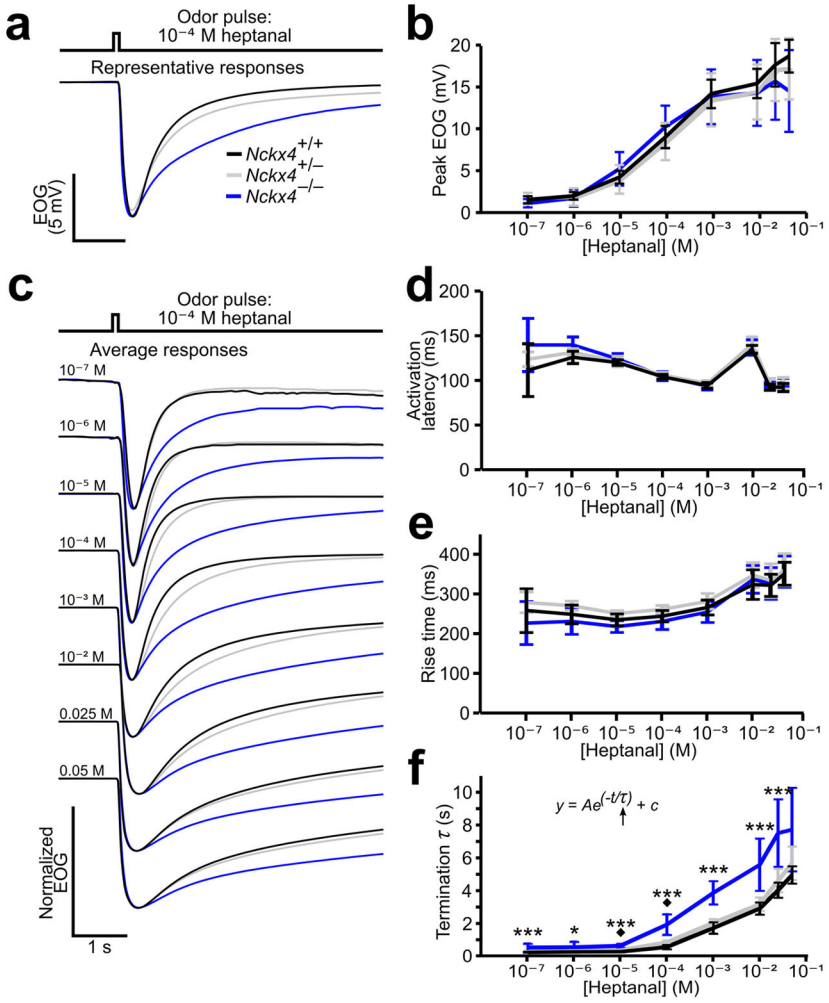

Figure 2. EOG analysis of *Nckx4*$^{-/-}$mice

(**a**) Representative EOG traces to a 100 – msec pulse of 10 $^{-4}$ M heptanal. The trace color codes also apply to (b) – (f).

(**b**) Dose – response relationships of EOG peaks evoked by single, 100 – msec pulses of heptanal. For (b) – (e), WT, n = 9 animals; *Nckx4*$^{+/-}$, n = 10; *Nckx4*$^{-/-}$, n = 7.

(**c**) Averaged EOG traces to a 100 – msec pulse of 10 $^{-7}$ – 0.05 M heptanal. The traces were normalized relative to their peaks to allow comparison of activation and termination kinetics.

(**d**) EOG activation latency, defined as the time from odor stimulation to 1% peak amplitude.

(**e**) EOG rise time, defined as the time from 1% to 99% peak amplitude.

(**f**) EOG termination rates. The termination time constant (τ) is determined by fitting a single exponential function to the termination phase of the EOG trace. For odor concentrations of 10 $^{-4}$ M and 10 $^{-3}$ M, n = 16 for WT, n = 19 for *Nckx4*$^{+/-}$, and n = 17 for *Nckx*$^{-/-}$. For other concentrations, n = 9 for WT, n = 10 for *Nckx4*$^{+/-}$, and n = 9 for *Nckx4*$^{-/-}$. Error bars, 95% CI. Asterisks indicate P values for WT vs. *Nckx4*$^{-/-}$(*, $P < 0.05$; ***, $P < 0.001$), and diamonds indicate P values for WT vs. *Nckx4*$^{+/-}$(◆, $P < 0.05$).

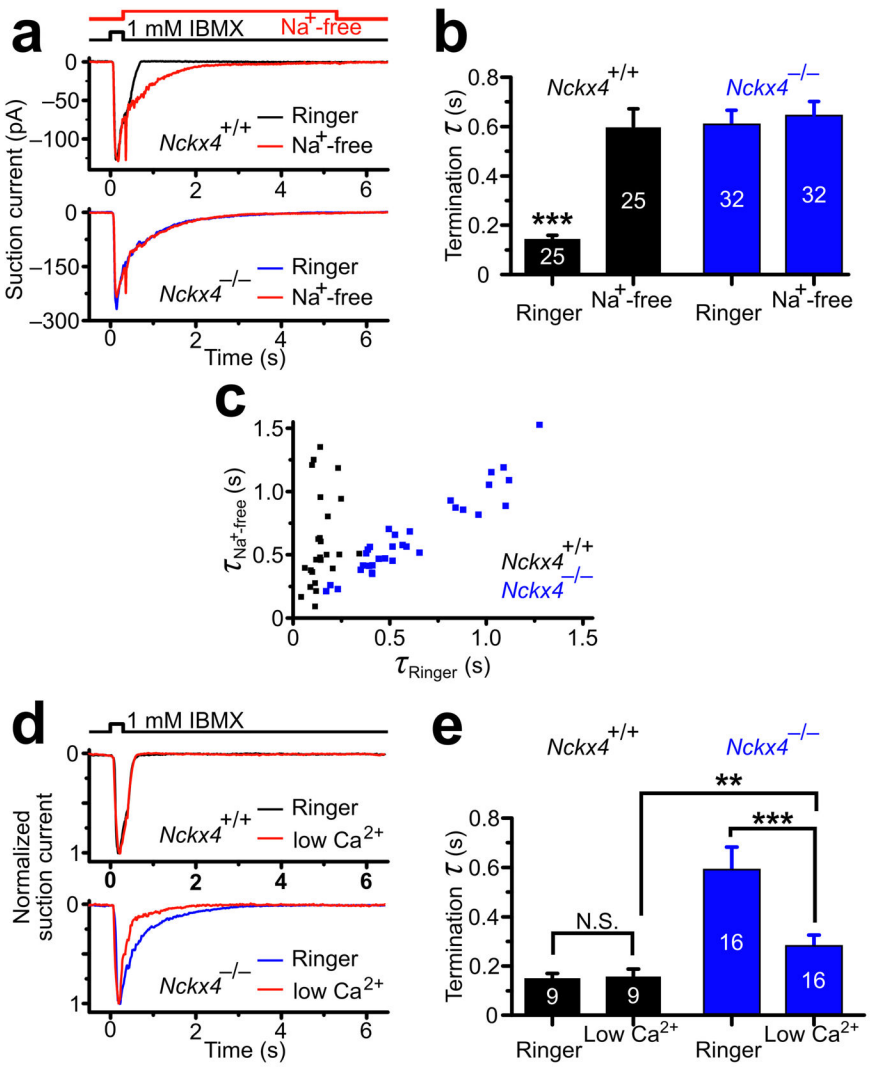

Figure 3. Single–cell analysis of Na^+/Ca^{2+} exchanger–dependent response termination

(**a**) Single cell suction electrode recordings from a dissociated WT (top panel) and *Nckx4*$^{-/-}$ (bottom panel) OSN stimulated with a 0.3–sec pulse of IBMX. For each neuron, two recordings were performed: one with extracellular Ringer's solution applied throughout the recording time period (black trace for WT, red trace for *Nckx4*$^{-/-}$), the other with a Na^+–free Ringer's solution applied during the termination phase of the OSN response (blue traces).

(**b**) Termination time constants (see Methods). Error bars represent s.e.m. ***, $P < 0.001$ for WT in Ringer's solution vs. all other categories. Cell numbers (*n*) are indicated within the bars.

(**c**) Plot of the termination time constants in a Na^+–free Ringer's solution vs. in a standard Ringer's solution for WT (black squares) and *Nckx4*$^{-/-}$ (red squares) OSNs. Each data point represents a single neuron.

(**d and e**) Ca^{2+} dependency of termination rates in *Nckx4*$^{-/-}$OSNs. (**d**) Recordings from a WT (top panel) and *Nckx4*$^{-/-}$ (bottom panel) OSN stimulated with a 0.3–sec pulse of

IBMX. For each neuron, two recordings were performed: one in standard Ringer solution (containing 2 mM Ca^{2+}), the other in low Ca^{2+} Ringer solution (containing 20 μM Ca^{2+}). The traces were normalized relative to their peaks for comparison of response kinetics. (**e**) The termination time constants are plotted for each genotype and condition. Error bars represent s.e.m. N.S., not significant; **, $P < 0.01$; ***, $P < 0.001$. Cell numbers (*n*) are indicated within the bars.

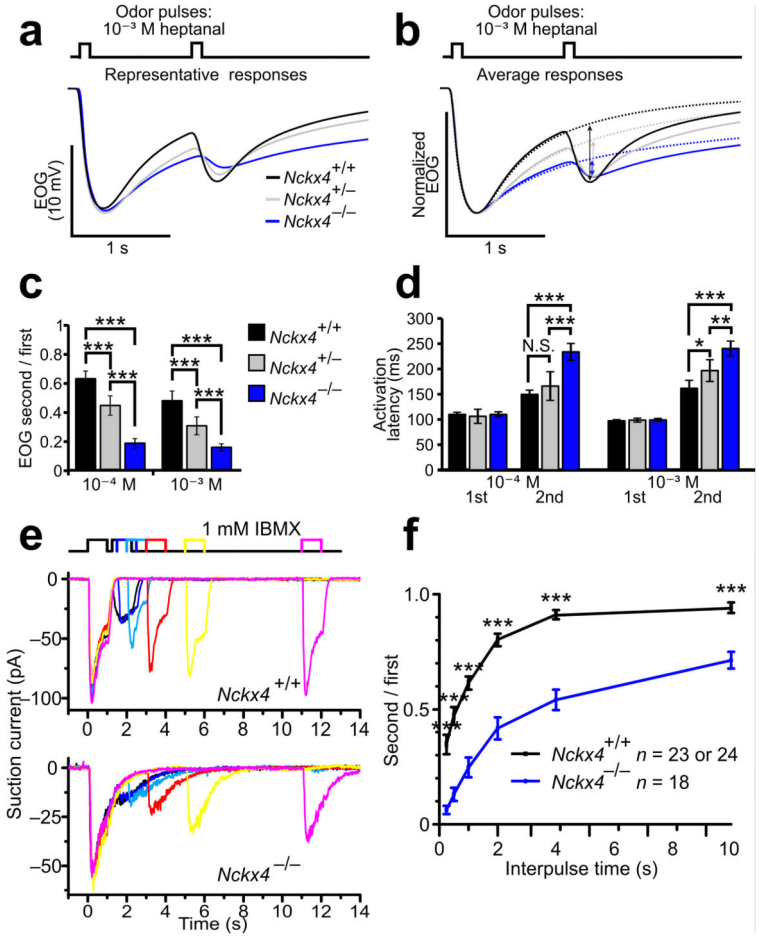

Figure 4. Analysis of adaptation of *Nckx4*$^{-/-}$OSNs

(**a–d**) EOG analysis of paired–pulse stimulation to heptanal (n = 10 animals for each genotype).

(**a**) Representative EOG traces.

(**b**) Solid traces depict averaged EOG recordings to paired–pulse stimulation. Dotted traces depict averaged EOG recordings to a single 100–msec pulse, which were used as the baseline for calculating the net amplitudes (indicated by the vertical bidirectional arrows) of the adapted responses in (c). The traces were normalized relative to the first EOG peak.

(**c**) Amplitude ratios of the second (adapted) response relative to the first. The amplitude of the second response is calculated by subtracting the single pulse recording from the paired–pulse recording for each animal. Error bars, 95% CI. ***, $P < 0.001$.

(**d**) Response latencies. The latency for the second pulse was calculated by subtracting the single pulse recording from the paired–pulse recording for each animal, and calculating the time from the second stimulation to 1% peak of the resulting trace. Error bars, 95% CI. N.S., not significant; *, $P < 0.05$; **, $P < 0.01$; ***, $P < 0.001$.

(**e** and **f**) Single–cell suction electrode recording analysis. (**e**) Recordings from a WT (upper panel) and a *Nckx4*$^{-/-}$ (lower panel) OSN stimulated with paired 1–sec pulses of 1 mM IBMX with varying interpulse intervals.

(**f**) Average amplitude ratios of the second response relative to the first, plotted against the interpulse time. Error bars represent s.e.m. ***, $P < 0.001$.

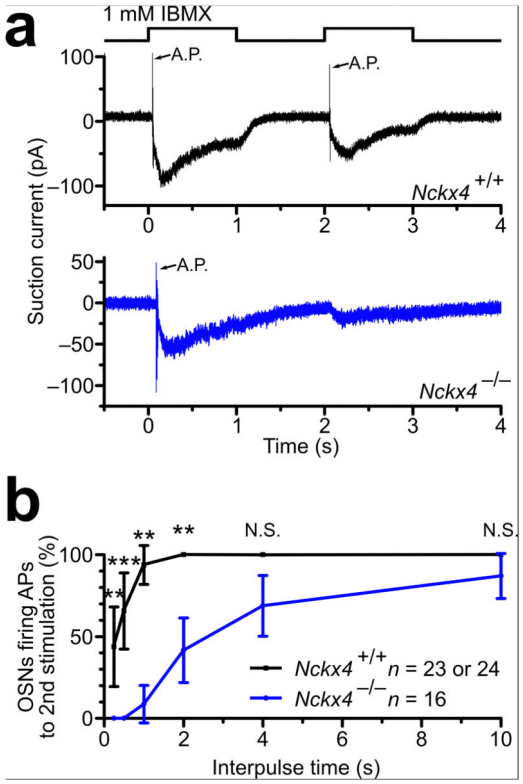

Figure 5. Single–cell analysis of action potential generation in *Nckx4*$^{-/-}$ OSNs

(**a**) Single–cell suction electrode recordings from a *Nckx4*$^{+/+}$ (upper panel) and a *Nckx4*$^{-/-}$ (lower panel) OSN stimulated with paired 1–sec pulses of 1 mM IBMX separated by a 1–sec interval. Traces were filtered with the wide bandwidth of DC – 5000 Hz to monitor action potential firing. Action potential currents (A.P.) are indicated by arrows.

(**b**) Percentage of OSNs firing action potentials, plotted against the interpulse time. Error bars, 95% CI. N.S., not significant; **, $P < 0.01$; ***, $P < 0.001$.

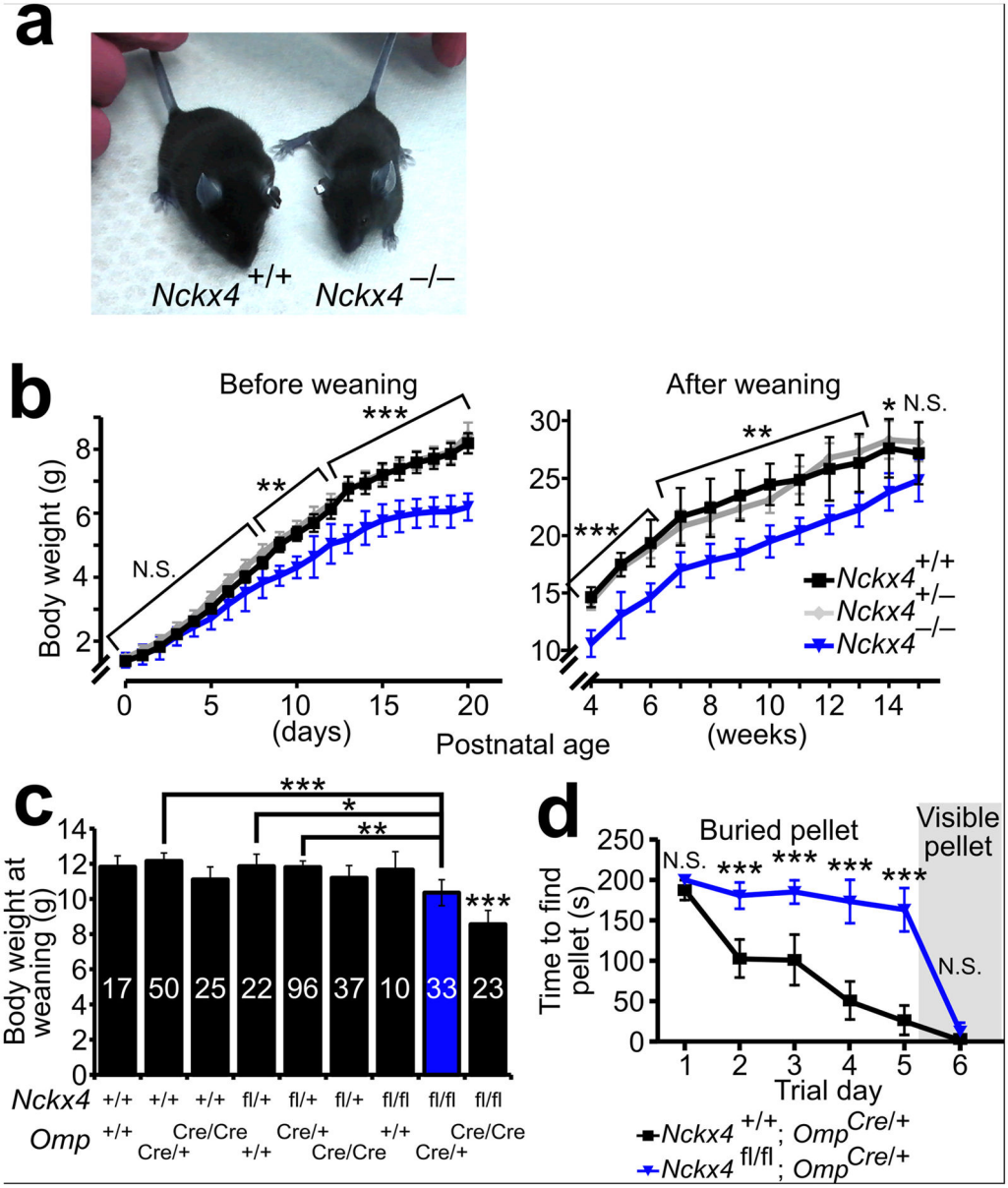

Figure 6. Effects of NCKX4 loss on olfactory–mediated behaviors

(**a**) Body size of a *Nckx4*$^{-/-}$ mouse relative to a *Nckx4*$^{+/+}$ mouse at 24 days postnatal age.

(**b**) Timecourse of average body weights for *Nckx4*$^{+/+}$ (n = 10–54), *Nckx4*$^{+/-}$ (n = 17–85), and *Nckx4*$^{-/-}$ (n = 5–31) mice before (left) and after (right) weaning. Error bars, 95% CI. Statistical significance for *Nckx4*$^{+/+}$ vs. *Nckx4*$^{-/-}$ is indicated over each timepoint: N.S., not significant; *, $P < 0.05$; **, $P < 0.01$; ***, $P < 0.001$.

(**c**) Average body weights for mice of all combinations of *Nckx4* (+ or flox) and *Omp* (+ or Cre) alleles at 24 days postnatal age. The red color highlights the olfactory conditional *Nckx4* knockout (*Nckx4*$^{flox/flox}$;*Omp*$^{Cre/+}$). Error bars, 95% CI. All genotypes weighed significantly more than the double knockout ($P < 0.001$). All other pairwise P–values that

are less than 0.05 are also indicated: *, $P < 0.05$, **, $P < 0.01$; ***, $P < 0.001$. Mouse numbers (*n*) are indicated within the bars.

(**d**) Buried Food Pellet Test for *Nckx4*$^{+/+}$;*Omp*$^{Cre/+}$ and *Nckx4*$^{flox/flox}$;*Omp*$^{Cre/+}$ mice (*n* = 20 mice per genotype). The average time to locate the food pellet is plotted against the trial day. On day 6, the pellet was left on the surface of the bedding to be visible to the mouse. Error bars, 95% CI. N.S., not significant; ***, $P < 0.001$. See Supplementary Movie 1 for a video of both genotypes' behavior in this task.